Photocatalytic degradation of methyl orange mediated by a silica coated nanomagnet porphyrin hybrid

Kelly A.D.F. Castro,[1,#,*] João M.M. Rodrigues,[2,#,*] M. Amparo F. Faustino,[1] João P.C. Tomé,[3] José A.S. Cavaleiro,[1] Maria da Graça P.M.S. Neves,[1,*] Mário M.Q. Simões[1,*]

[1]*LAQV-REQUIMTE, Department of Chemistry, University of Aveiro, 3810-193 Aveiro, Portugal*
[2]*CICECO - Aveiro Institute of Materials, Department of Chemistry, University of Aveiro, 3810-193 Aveiro, Portugal*
[3]*Centro de Química Estrutural, Instituto Superior Técnico, Universidade de Lisboa, Av. Rovisco Pais, 1049-001 Lisboa, Portugal*

*Corresponding authors: Kelly A.D.F. Castro (kadfc16@gmail.com), João M.M. Rodrigues (jrodrigues@ua.pt), Maria da Graça P.M.S. Neves (gneves@ua.pt), Mário M.Q. Simões (msimoes@ua.pt)

Abstract

The photocatalytic activity of a silica coated nanomagnet porphyrin hybrid (**NPH**) and of the corresponding porphyrin precursors (**H_2P** and **ZnP**) was evaluated in the degradation of the methyl orange dye (**MO**) under visible light irradiation. The catalytic degradation of **MO** was performed under air, in the absence and in the presence of aqueous hydrogen peroxide. The results show that the hybrid **NPH** was the most effective photocatalyst causing the total degradation of **MO** after 270 min of irradiation in the presence of hydrogen peroxide. The remarkable photocatalytic activity of this **NPH**, associated with the possibility of reuse, makes this material a promising photocatalyst.

Keywords: *porphyrin, silica nanomagnetic particles, photocatalysis, methyl orange, degradation.*

[#]*These two authors contributed equally to this work*

Introduction

Environmental pollution is one of the major and most urgent problems of the modern world requiring a constant and special attention from the scientific community. In particular, wastewater from dyeing industries has become exceptionally worrisome, since the presence of dyes can inhibit sunlight penetration and, consequently, reduce the photosynthetic process [1, 2]. Following these inputs, the scientific community is contributing with the development of novel and economically sustainable methodologies for the detoxification of textile wastewaters, aiming to respect the recommended quality criteria and thus close the water cycle [3, 4].

The large-scale use of dyes results in the production of large volumes of pollutants, which are often discarded without any previous treatment. Therefore, the development of efficient methodologies in order to minimize the environmental impact caused by industrial effluents is of great interest [5]. Different methodologies have been developed for the degradation and/or scavenging of those dyes, especially azo dyes (the most common synthetic dyes, ca 70% wt.). These methodologies include adsorption, biological oxidation, membrane filtration, ozonation, oxidation using UV/H_2O_2, UV/TiO_2 and UV or visible light and catalysis [3, 6-9]. The approaches based on catalytic processes appear as important alternatives in the remediation of effluents. In fact, the fundamental pillar of green chemistry is catalysis, generally resulting in significant gains in terms of overall efficiency of a chemical reaction. Porphyrins and analogues are among the catalysts with recognized efficacy for azo dyes degradation [5, 10].

Metalloporphyrins and analogues have already proved their efficiency as catalysts, namely for oxidative reactions [11-20]. Porphyrins are also efficient producers of reactive oxygen species (ROS) in the presence of light, such as singlet oxygen ($^1O_2$) [21-24], thus inducing many photocatalytic reactions [25, 26]. The reaction of ROS with the target pollutants is an alternative method for removing organic pollutants [27, 28]. From the successful history of photocatalysts, the special attention given to porphyrins and analogues by the scientific community is due to their strong absorption bands in the visible region, versatile chemical structures, and facile tuning of the electronic properties. Besides, the insertion of diverse metals into the core of the macrocycle can

modulate the catalytic activity associated with the porphyrins' structure. Additionally, the development of heterogeneous catalysts based on porphyrins represents an important challenge for a sustainable development.

Recently, magnetite nanoparticles (Fe_3O_4) have aroused great interest due to their physicochemical characteristics. Fe_3O_4 with different structures has been used in different areas, such as environmental technology, nanotechnology, medicine and catalysis [29-33]. In addition to their exceptional variety of applications, magnetite nanoparticles have the advantage of reuse. For instance, Qin and co-workers studied Fe_3O_4/TiO_2 magnetic nanoparticles for photocatalytic degradation of phenol [34]. Kim and co-workers reported the synthesis and characterization of magnetic nanoparticles functionalized with [5,15-bis(phenyl)-10,20-bis(4-methoxycarbonylphenyl)porphyrin]platinum(II) and studied the photocatalytic activity of this material using 2,4,6-trichlorophenol as the target pollutant [35]. More recently, magnetite nanoparticles with different morphologies (cubic-shaped and spherical) decorated with the 5,10,15,20-tetrakis(4-carboxyphenyl)porphyrin showed to be able to generate $^1O_2$ under ultraviolet irradiation. Their study as photocatalysts towards bisphenol A (BPA) disclosed degradation values of 64% (cubic-shaped) and of 90% (spherical shape) in the presence and absence of hydrogen peroxide (H_2O_2) [36]. Additionally, these materials retained their catalytic features for at least three catalytic cycles.

Following our interest in developing new materials for environmental remediation, in this communication we report the synthesis and characterization of core-shell magnetite-silica nanoparticles functionalized with the Zn(II) complex of a porphyrin obtained from the reaction of 5,10,15,20-tetrakis(pentafluorophenyl)porphyrin with tosylethylenediamine. Furthermore, the efficacy of this material to act as photocatalyst was evaluated under visible white (380-800 nm) light irradiation using methyl orange dye (**MO**) as the target pollutant. The studies were performed under air in the absence and in the presence of aqueous H_2O_2.

Experimental

Reagents and Equipment

All chemicals used in this study were purchased from Sigma-Aldrich or Merck and were of analytical grade.

Electronic spectra (UV-Vis) were obtained on a Shimadzu UV-2501PC spectrophotometer, in the 350-800 nm range. The fluorescence emission spectra were recorded in DMF in 1 x 1 cm quartz optical cells at 298 K under normal atmospheric conditions on a computer controlled Horiba Jobin Yvon FluoroMax-3 spectrofluorimeter. The widths of both excitation and emission slits were set at 2.0 nm. ^{1}H, ^{19}F and ^{13}C NMR spectra were recorded on a Bruker Avance AMX 300 spectrometer at 300.13, 282.38 and 75.47 MHz, respectively. Deuterated dimethylsulfoxide was used as solvent and TMS (δ = 0 ppm) as the internal standard; chemical shifts are reported in ppm (δ) and coupling constants (*J*) are given in Hz. Mass spectra were acquired on an Applied Biosystems Analyzer mass spectrometer (MALDI TOF/TOF). HRMS-ESI spectra were recorded on VG AutoSpec-M spectrometer.

*Preparation of porphyrins **H_2P** and **ZnP***

The porphyrins were prepared according to the following steps:

i) The precursor 5,10,15,20-tetrakis(pentafluorophenyl)porphyrin **[H_2(TPFPP)]** was synthesized by condensation of pyrrole with pentafluorobenzaldehyde under acidic conditions [11, 37].

ii) The tri-substituted free-base porphyrin (**H_2P**) was obtained by structural modification of **[H_2(TPFPP)]** in the presence of the nucleophile *N*-tosylethylenediamine, as described in the literature [38].

iii) Zinc(II) acetate (42.1 mg, 0.32 mmol) was added to a solution of **H_2P** (50.0 mg) in dichloromethane/methanol (2:1, 15 mL) and the resulting mixture was refluxed at 60 ºC for 1 h (Scheme 1). After cooling to room temperature, the reaction mixture was washed with distilled water. The organic phase was dried (Na_2SO_4) and the solvent was evaporated under reduced pressure. The **ZnP** was obtained in quantitative yield by crystallization in dichloromethane/hexane.

H_2P: Yield: 19%; **^{1}H NMR** (DMSO-d_6): δ -3.13 (s, 2H, NH), 2.37 (s, 9H, Ts-CH_3), 3.18 (q, *J* = 6.2 Hz, 6H, CH_2), 3.64 (q, *J* = 6.2 Hz, 6H, CH_2), 6.47 (s, 3H, NH-PhF_4), 7.47 (d, *J* = 8.2 Hz, 6H, Ts-*o*-H), 7.81 (d, *J* = 8.2 Hz, 6H, Ts-*m*-H), 7.90 (t, *J* = 6.1 Hz, 3H, NH-Ts), 9.24-9.33 (m, 8H, H-β) ppm. **^{19}F NMR** (DMSO-d6): δ -163.03 (dd, *J* = 26.4 and 5.3 Hz, 2F, *o*-F), -166.67 (d, *J* = 18.4 Hz, 6F, -Ts-*o*-F), -177,52 (t, *J* = 22.4 Hz, 1F, *p*-F), -183.67 to -183.77 (m, 6F, Ts-*m*-F), -186.35 (dd,

J = 33.9 and 14.4 Hz, 2F, *m*-F). **UV-Vis** ($CHCl_3$), λ_{max}: (log ε): 421 (5.36), 511 (4.26), 548 (3.64), 586 (3.86), 653 (3.42). **UV-Vis** (DMSO), λ_{max}: 424, 512, 548, 586, 648 nm. **HRMS-ESI:** Calculated for $C_{71}H_{50}F_{17}N_{10}O_6S_3$ $[M+H]^+$ 1557.2805; found: 1557.2587.

ZnP: **^{1}H NMR** (DMSO-d_6): δ 2.36 (s, 9H, Ts-CH_3), 3.16 (q, *J* = 6.0 Hz, 6H, CH_2), 3.61 (q, *J* = 6.0 Hz, 6H, CH_2), 6.39 (s, 3H, NH-PhF_4), 7.47 (d, *J* = 8.2 Hz, 6H, Ts-*o*-H), 7.81 (d, *J* = 8.2 Hz, 6H, Ts-*m*-H), 7.91 (t, *J* = 6.0 Hz, 3H, NH-Ts), 9.07-9.16 (m, 8H, *β*-H). **^{19}F NMR** (DMSO-d_6): δ -162.78 to -162.87 (m, 2F, *o*-F), -166.22 (d, *J* = 17.8 Hz, 6F, *o*-F), -178.23 (t, *J* = 22.4 Hz, 1F, *p*-F), -184.06 (dd, *J* = 17.8 and 10.1 Hz, 6F, *m*-F-Ts), -186.73 to -186.92 (m, 2F, *m*-F). **UV-Vis** ($CHCl_3$), λ_{max} (log ε): 418 (5.24), 513 (4.24), 580 (3.43) nm. **UV-Vis** (DMSO), λ_{max}: 420, 520, 586 nm. **MS (MALDI TOF/TOF)** (*m/z)*: 1620.0 $[M+H]^+$.

*Preparation of the Nanomagnet Porphyrin Hybrid (**NPH**) material*

The Nanomagnet Porphyrin Hybrid **(NPH)** material was prepared according to the procedure described in the literature [39]. Briefly, the magnetic core (magnetite) was synthesized by the co-precipitation method under basic conditions using ammonium hydroxide. In the second step, the magnetite was coated with silica using the silicic acid method. In the third step, the nanoparticle was maintained under stirring for 24 h in the presence of (3-aminopropyl)triethoxysilane (APTS) in order to obtain the nanoparticle functionalized with aminopropyl chains. The magnetic aminopropyl silica nanoparticles (**Si-NP**) were isolated and then washed several times with ethanol, followed by purification by magnetic decantation. Subsequently, the immobilization of the porphyrin **ZnP** into **Si-NP** was performed. For this, a previously prepared ethanol suspension of the **Si-NP** [39] (13.5 mL, corresponding to 250 mg of Si-NP) were filtered through a polyamide membrane, washed several times with DMSO and re-suspended in DMSO (6 mL). A solution of **ZnP** (20.0 mg, 12.3 μmol) in DMSO (2 mL) was added to the previous **Si-NP** suspension and the resulting mixture was stirred for 24 h at 160 °C (Scheme 1). The immobilization of **ZnP** was monitored by thin-layer chromatography: the spot corresponding to **ZnP** decreases progressively while the spot corresponding to the **NPH** material (at the application point) increases. The insoluble material with

a violet color was washed several times with appropriate solvents: firstly dichloromethane and then a mixture of dichloromethane/methanol (90:10) until the Soret band of the **ZnP** was no longer detected through UV-Vis in the rinsing solvent. The quantification of the **ZnP** present in the washing solvent allowed to calculate the **ZnP** loading in the material (based on the ε value of the Soret band of ZnP). In the washing process, the hybrid material **NPH** was firstly decanted on a magnet field and then filtered under vacuum, using a polyamide membrane on a Büchner funnel. The **NPH** material was re-suspended and kept in dry DMSO (25 mL), making a stock solution of the **NPH** photocatalyst for the photocatalytic activity assays. **NPH** was characterized by UV-Vis and fluorescence spectroscopy.

Singlet oxygen generation

Stock solutions of each porphyrin (**H_2P** and **ZnP**) and of 1,3-diphenylisobenzofuran (DPiBF) in DMF at 0.1 mM and 10 mM, respectively, were prepared. The reaction mixture containing DPiBF (50 μM) and a solution of each photocatalyst (0.5 μM) in DMF was irradiated in a quartz cell (3 mL), under magnetic stirring at an irradiance of 10 $mW.cm^{-2}$ with a homemade LEDs array. The LEDs array is composed of a matrix of 5 x 5 LEDs making a total of 25 light sources with an emission peak centered at 654 nm and a bandwidth at half maximum of ± 20 nm. During the irradiation period the solutions were stirred at ambient temperature. The DPiBF degradation was monitored by measuring the absorbance decrease at 415 nm at irradiation intervals of 1 min. The percentage of decay of DPiBF absorption is related with the production of singlet oxygen. The quantification was achieved by the difference between the initial and the final absorbance at 415 nm over a given irradiation time. The same strategy was adopted for **NPH**, but the PS concentrations used were 0.5, 1.0, 2.0, and 5.0 μM. The results obtained were compared with those obtained in the presence of **H_2TPP** (5,10,15,20-tetraphenylporphyrin) and in the absence of any porphyrin (negative control) under similar irradiation conditions.

Photocatalytic activity

The photocatalytic activity of **H_2P**, **ZnP** and **NPH** was evaluated in aqueous solutions using methyl orange (**MO**) as model substrate and under visible light

irradiation, which was performed with a halogen 500 W lamp at an irradiance of 150 mW cm^{-2}. This light source was positioned 10 cm away from the batch reactor and the temperature was kept at *ca* 20 ºC. The reactions were performed under air and in the presence of aqueous H_2O_2. A stock solution of the dye ([**MO**] = 8.26 × 10^{-2} mol L^{-1}) was prepared in milli-Q water. To a 4 mL quartz cuvette, 3.0 mL of water, 200 µL of **MO** dye solution and the adequate volume of stock solution of the catalyst (**H_2P** or **ZnP**) to obtain a final concentration of 0.5 µM in DMSO were added. For the reactions carried out in the presence of hydrogen peroxide, 100 µL of aqueous H_2O_2 (30%, w/w) were added. In the case of the heterogeneous photocatalyst (**NPH**), the solution was stirred in the dark (30 min) before irradiation in order to obtain an equilibrium point of initial physical adsorption of **MO** over the surface of the photocatalyst. All photocatalytic experiments were accomplished under similar conditions. The photocatalytic performance was monitored indirectly by relating the decrease in the absorbance of **MO** at 464 nm in solution with its degradation. The photocatalytic reactions in the presence of hydrogen peroxide were also performed in the presence of mannitol.

Results and Discussion

Synthesis and characterization of the photocatalysts

The synthetic methodology used in the preparation of the homogeneous and the heterogeneous photocatalysts is summarized in Scheme 1. The porphyrin derivative **H_2P** was prepared by a controlled nucleophilic substitution of three of the *p*-fluorine atoms in **H_2(TPFPP)** with *N*-tosylethylenediamine, according to the procedure reported previously by our investigation group [38]. The subsequent metalation with zinc(II) ions of the inner core of **H_2P** was performed in dichloromethane:methanol at 60 ºC using zinc(II) acetate (Scheme 1). The structural confirmation of **H_2P** and **ZnP** was performed by ^{1}H NMR, mass spectrometry (Figs. S1-S4 in the Supporting information) and UV-Vis spectroscopy.

The covalent immobilization of **ZnP** onto the core-shell magnetite silica nanoparticles (**Si-NP**) functionalized with amino groups occurred via nucleophilic substitution of the *p*-fluorine atom at the C_6F_5 group. The functionalized nanoparticles **Si-NP** were obtained by treating the magnetic core (obtained by the co-precipitation approach) covered with silica with APTS [39, 40]. The

immobilization of the **ZnP** was performed in DMSO at 160 ºC for 24 h. After this period, a violet insoluble nanoparticles was isolated and washed several times with appropriate solvents to afford the desired **NPH**. The rinsing solutions resulting from the washing process were collected and analyzed by UV-Vis in order to quantify the loading of **ZnP** in the solid material nanoparticles (**NPH**). Then, **NPH** was re-suspended in DMSO and was also characterized by UV-Vis and fluorescence spectroscopy [39, 40].

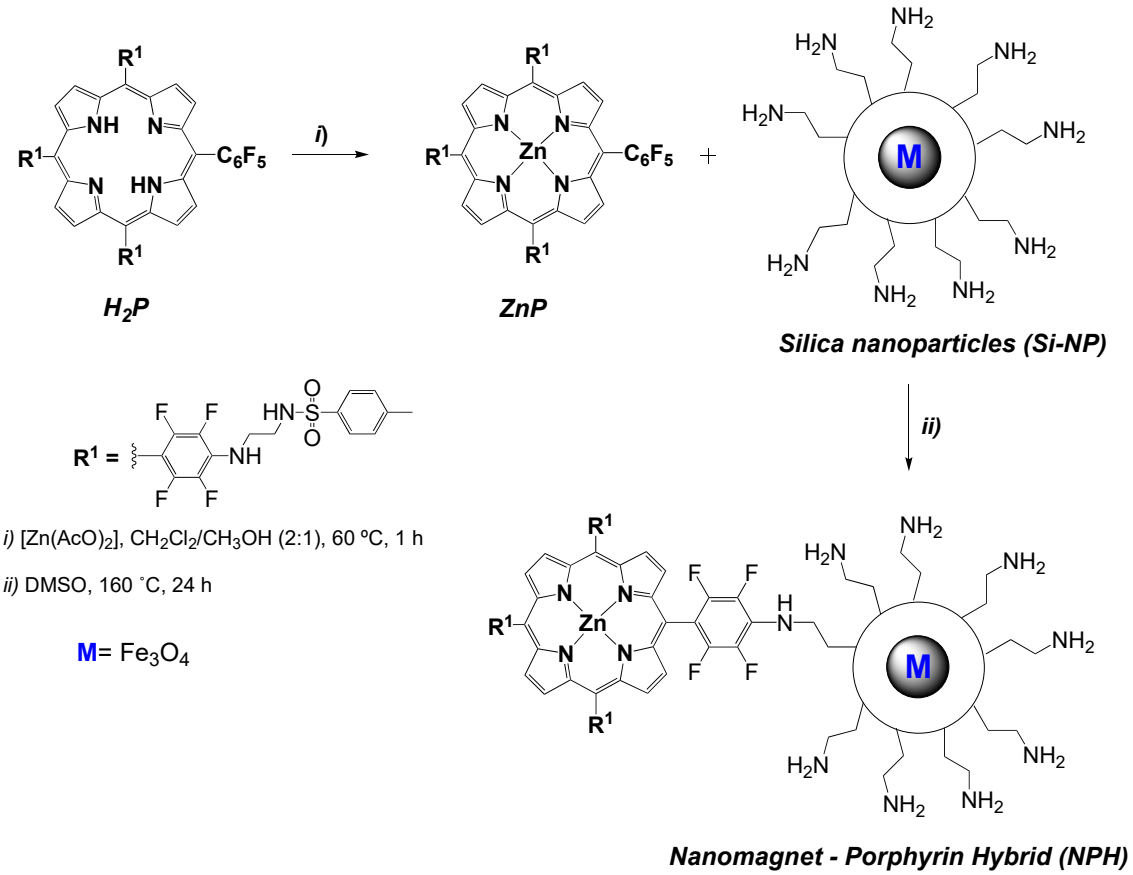

Scheme 1. Synthetic procedure used to obtain the Nanomagnet-Porphyrin Hybrid (**NPH**).

The UV-Vis spectra of **H₂P**, **ZnP** and of the **NPH** suspension in DMSO are displayed in Figure 1. The non-immobilized porphyrin derivatives **H₂P** and **ZnP** show the typical Soret band at 424 and 420 nm, respectively, accompanied by the less intense Q bands at 512, 548, 586, and 648 nm for **H₂P** and at 520 and 586 nm for **ZnP**; this decrease in the number of the Q bands after metalation is related to the alteration in the micro symmetry of the porphyrin macrocycle. The presence of **ZnP** on the magnetic nanoparticles **HNP** was promptly confirmed by the appearance of the Soret band at 419 nm and of the less intense Q-bands at

515 and 580 nm. These features validated the success of the immobilization and the UV-Vis spectrum profile is similar to that obtained for the non-immobilized **ZnP** in solution. The UV-Vis spectra of **ZnP** and **NPH** in the solid-state show the typical absorption Soret band at 430 nm (Supporting Information). Additionally, the UV-Vis spectra were also acquired in a mixture of DMSO:H_2O and are shown in the SI (Figure SXX). The spectrum of the silica nanoparticles (**Si-NP**) did not present bands in the region of 400 nm (Figure S4).

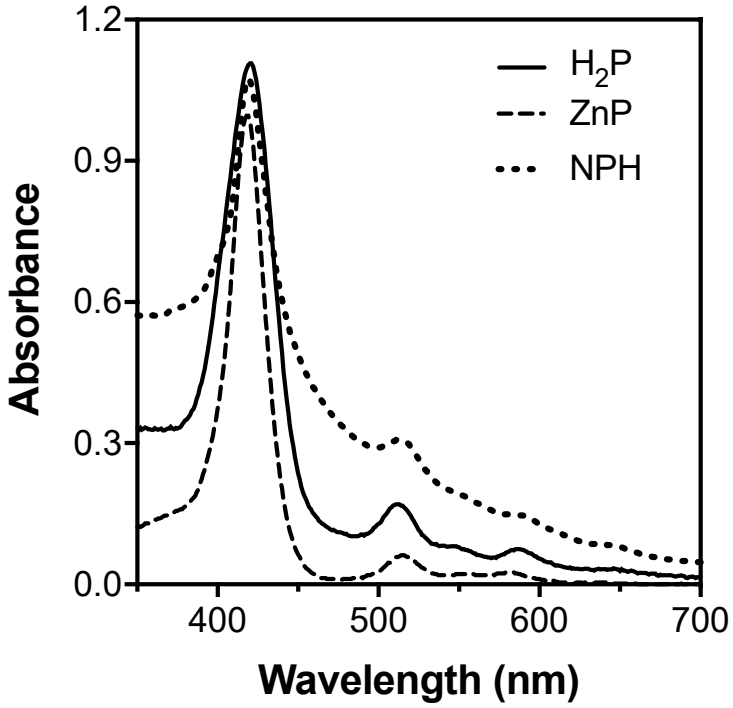

Figure 1. UV-Vis spectra of **H_2P**, **ZnP** and **NPH** in DMSO.

Upon excitation at 410 nm, the fluorescence emission spectrum of the **NPH** material in DMSO solution showed one strong emission band in the red region at *ca.* 600 nm [λ > Qx(0,0)]; the non-immobilized **ZnP** presents two bands in the red region at *ca.* 594 and 657 nm (data not shown). The **Si-NP** did not present emission bands upon 410 nm excitation, so the characteristic band of **NPH** can only be due to immobilized **ZnP** (Figure 2).

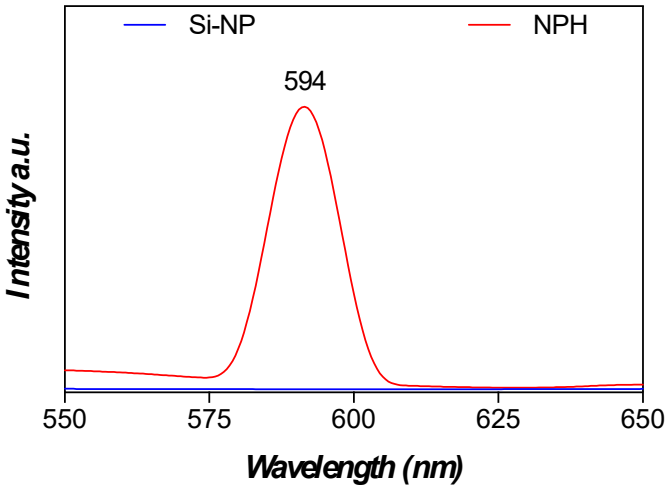

Figure 2. Emission spectra of **Si-NP**, **ZnP** and **NPH** in DMSO solution.

Singlet oxygen generation

The ability of photocatalysts to generate ROS, namely singlet oxygen ($^1O_2$), superoxide anion radical ($O_2^{\bullet-}$), hydrogen peroxide (H_2O_2) and hydroxyl radical ($^{\bullet}OH$) is a crucial parameter to be considered with regard to the efficiency of the photocatalyst.[41] In general, when porphyrin derivatives are used as photocatalysts, $^1O_2$ is the major ROS involved.[25] The production of $^1O_2$ was assessed by an indirect chemical method using 1,3-diphenylisobenzofuran (DPiBF) as a probe. This compound, as other furans, is able to react as a diene in a [4+2] process with $^1O_2$ as the dienophile, thus affording the colorless *o*-dibenzoylbenzene; with this quencher, exclusively $^1O_2$ is detected [42].

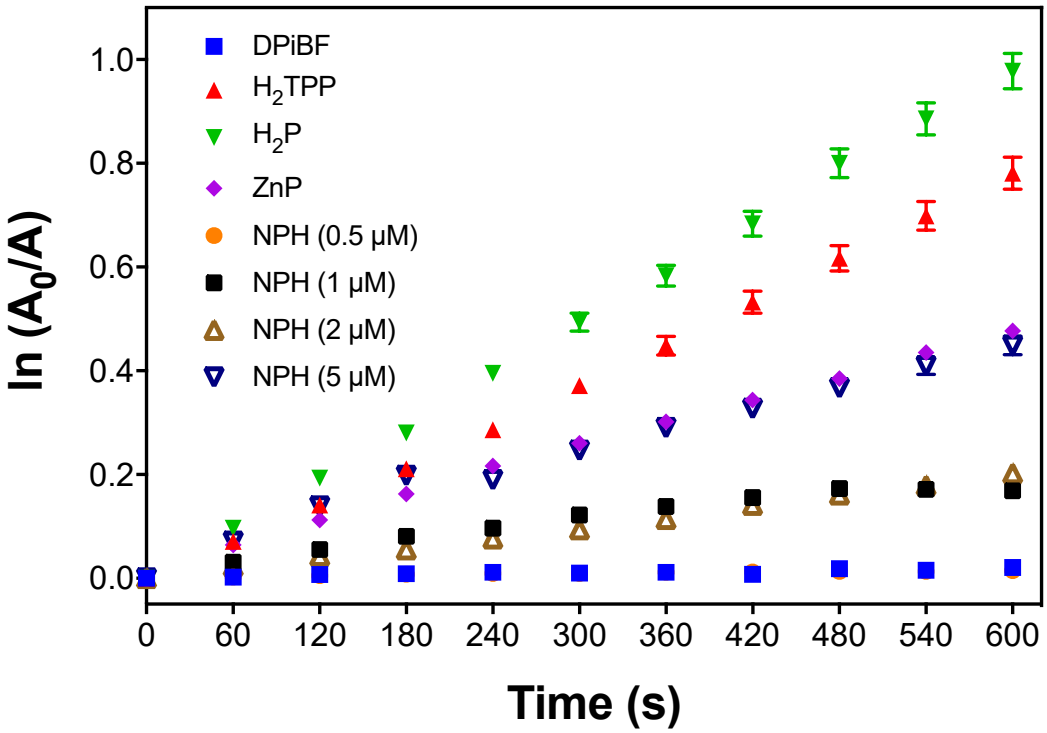

Figure 3. Time dependent photodecomposition of DPiBF (50 μM) mediated by **H_2P**, **ZnP** and **NPH** in DMF upon irradiation with red light (654 ± 20 nm) with or without porphyrin (0.5 μM for **H_2P** and **ZnP**) and 0.5, 1.0, 2.0 and 5.0 μM for **NPH**. **H_2TPP** was used as reference.

So, the photodegradation of DPiBF mediated by **H_2P**, **ZnP**, **NPH** and also by **H_2TPP** (used as reference) was qualitatively assessed by monitoring its absorbance decay at 415 nm as a function of the irradiation time with red light (654 ± 20 nm). The results in Fig. 3 show that the absorbance of DPiBF at 415 nm decreased in the presence of all porphyrin derivatives under irradiation as a function of time through a 1st order kinetic. Comparing the photodecomposition slope promoted by each porphyrin is observed that **H_2P** was the best $^1O_2$ generator, being even better than the reference (**H_2TPP**), followed by **ZnP** and **NPH**. For **NPH**, a significant increase of $^1O_2$ production was observed when its concentration was increased from 0.5 to 5 μM. This observation was important in order to establish the amount of material for the photocatalytic reactions. This reduction in $^1O_2$ production is in accordance with other studies involving silica nanoparticles or others nanoplatforms where the $^1O_2$ production by the porphyrin immobilized is significantly reduced [43].

Photocatalytic activity

The photocatalytic activity of **H_2P, ZnP** and **NPH** was evaluated using **MO** as an azo dye model due to its resistance to environmental degradation. The experiments were performed under visible light irradiation (380-800 nm) under air, and in the absence or in the presence of aqueous H_2O_2 as oxidant. The degradation of **MO** in the presence of **H_2P**, **ZnP** and **NPH** was monitored by measuring the decay of **MO** absorbance band at 464 nm. The photocatalytic efficiency of the different materials was expressed using the following equation: $(A_0-A_t)/A_0$, where A_0 is the absorbance of **MO** in the reaction mixture at time zero and A_t is the **MO** absorbance at an established time (t).

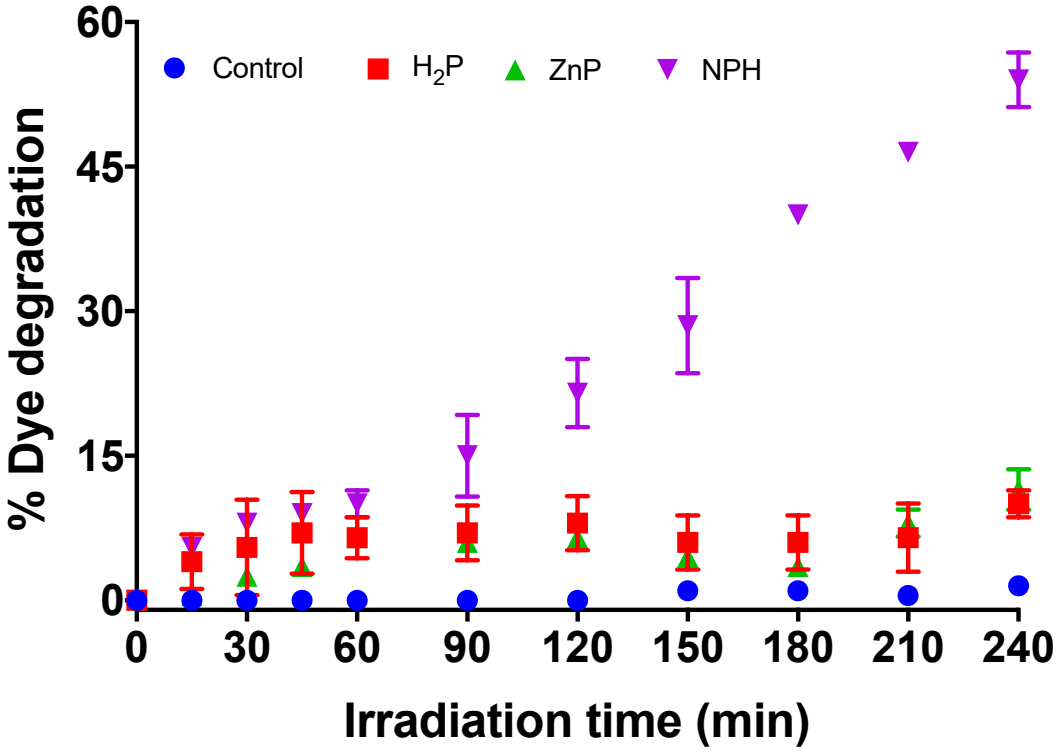

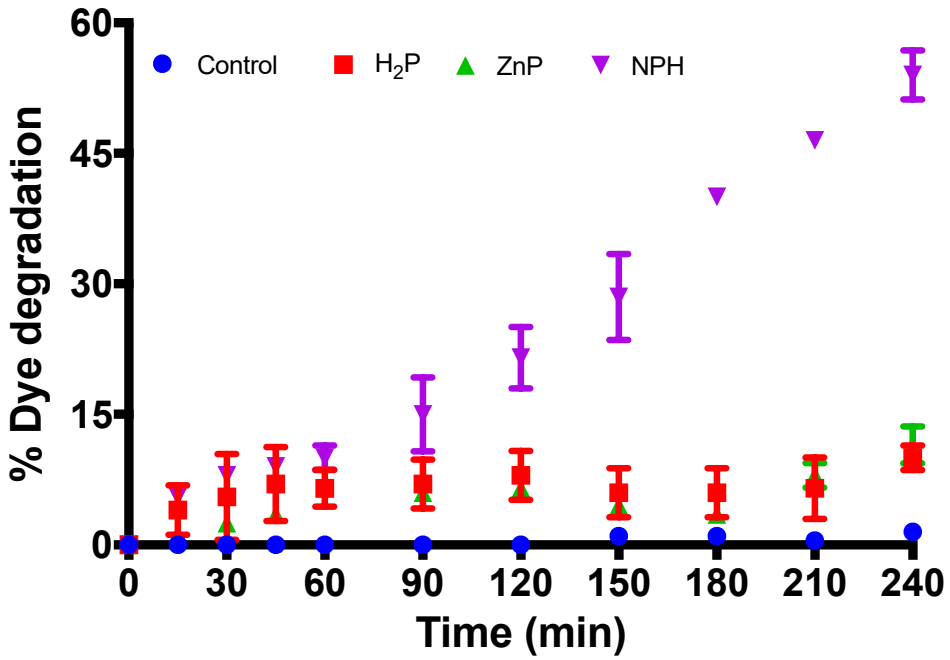

Figure 4. Photocatalytic degradation of methyl orange (**MO**) under air at different photoreaction times under white light irradiation (150 mW cm^{-2}): in the presence of 0.5 μM of **H_2P** (red shape) and **ZnP** (green shape); 5.0 μM of porphyrin immobilized in **NPH** (purple shape) and in the absence of catalyst (Control, blue shape). The absorption of **MO** was monitored at 464 nm.

The catalysts **H_2P**, **ZnP** and **NPH** showed significant differences ($p < 0.05$) in terms of dye degradation efficiency when the irradiations were performed without H_2O_2 (Figure 4). **NPH** was the most efficient photocatalyst causing a reduction of 54% in **MO** dye concentration after 240 min of irradiation when compared with **H_2P** and **ZnP** which attained a maximum of *ca* 12% under the same irradiation period.

The results obtained when the experiments were repeated in the presence of H_2O_2 are summarized in Figures 5 and 6, in the dark and after being irradiated, respectively. The results in Figure 5 show that in the absence of light (dark conditions) and after 90 min of reaction in the presence of any of the catalysts and H_2O_2 only 7% of **MO** was oxidized. After 270 min of reaction this value reached 13% for **ZnP** and **NPH** while for **H_2P** the value remain almost constant (*ca* 8%) and was similar to that observed for the control assay (reaction performed in the presence of H_2O_2 only). These results indicate that there is no remarkable difference between the different catalysts when dye degradation is performed in the presence of H_2O_2 but in the absence of light.

The results in Figure 6 show that the profile of these reactions in the presence of aqueous H_2O_2 are totally different when carried out under light irradiation. In fact, the action of light was particularly relevant for improving the rate of oxidation mediated by **NPH** (100% after 270 min) and **ZnP** (75% after 270 min). When compared with the photoreactions performed under light irradiation but in absence of H_2O_2 (Figure 3), an increment of *ca* 46% in catalytic activity was achieved for **NPH**, 56% for **ZnP** and 12.5% for **H_2P**. So, the beneficial effect of H_2O_2 in **MO** photodegradation is obvious when the results are compared with those obtained in the absence of H_2O_2 (Figures 4 and 6). The photodegradation of **MO** in the presence of **ZnP**, **NPH** and H_2O_2 showed to be time-dependent. This time dependence was also observed for **NPH** in the absence of H_2O_2. In fact, a longer contact time with the photocatalyst can facilitate the interaction of **MO** with the oxidation promoting species. The pathway responsible for **MO** photodegration after photocatalyst activation by white light in the presence of molecular oxygen (O_2) can involve ROS such as hydrogen peroxide, superoxide and hydroxyl radicals (type I photochemical pathway) and/or singlet oxygen (photochemical pathway type II). Additionally, the decomposition of H_2O_2 through a Fenton-like reaction can be facilitated in the presence of **NPH** affording hydroxyl radicals [44]. The results show that the photocatalytic activity of **H_2P, ZnP** and **NPH** cannot be justified only by their efficiency to produce $^1O_2$ (**H_2P** > **ZnP** > **NPH**) and probably other highly reactive species such as hydroxyl radical ($^{\bullet}$OH) are also involved. In order to verify if the production of $^{\bullet}$OH is also involved in the photocatalytic degradation of **MO**, the reactions in the presence of H_2O_2 were carried out in the presence of mannitol, an effective radical scavenger for $^{\bullet}$OH [45] (Figure 7).

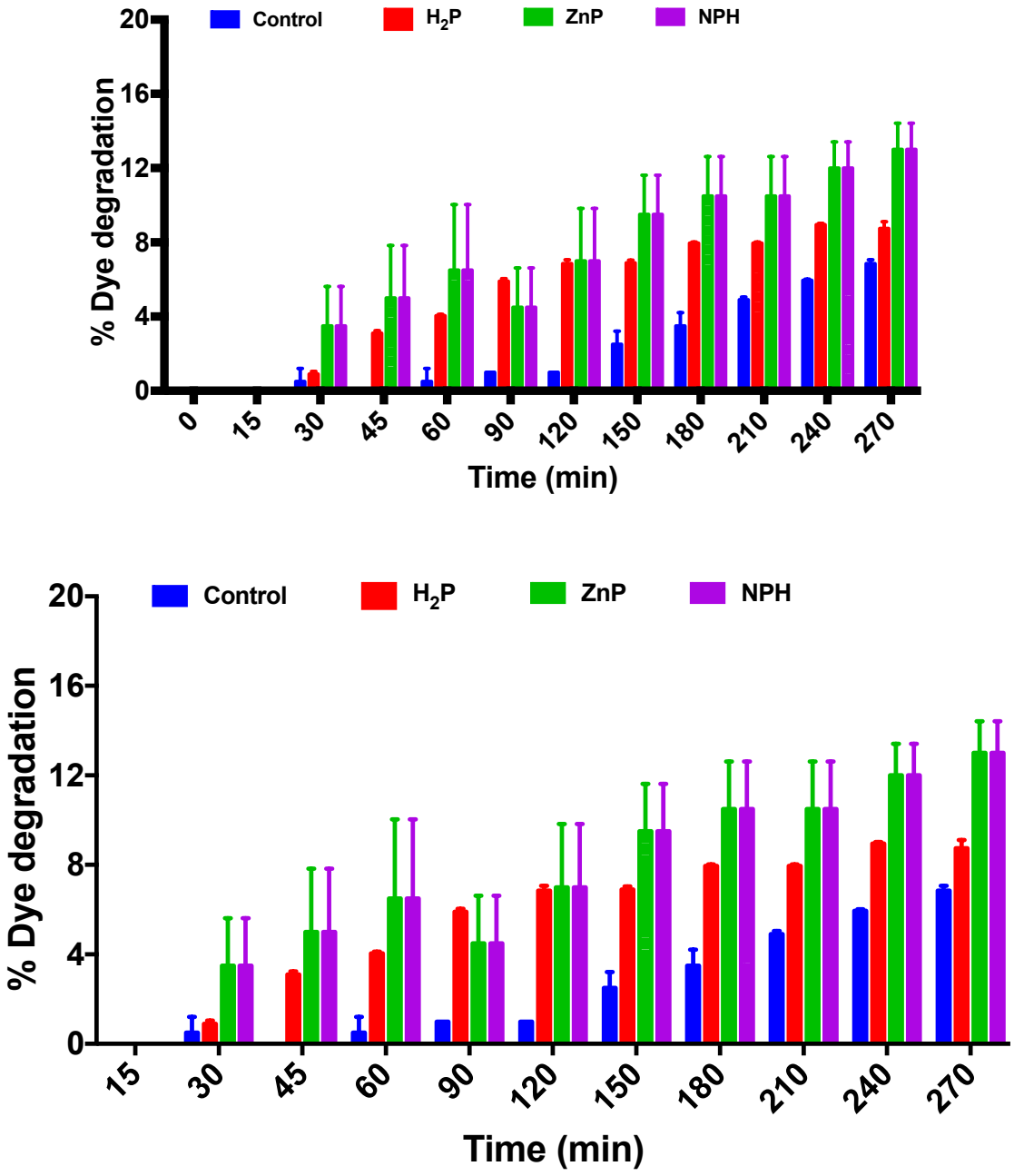

Figure 5. Degradation of methyl orange (**MO**) under dark conditions at different reaction times: in the presence of hydrogen peroxide and **H_2P** (red bars); **ZnP** (green bars); **NPH** (purple bars) and with no catalyst (Control, blue bars). The **MO** absorbance was monitored at 464 nm.

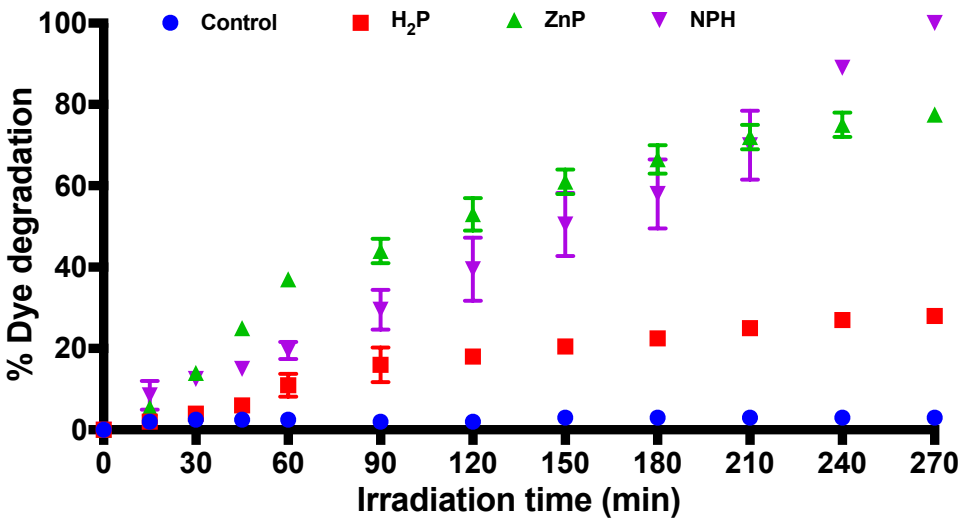

Figure 6. Photocatalytic degradation of methyl orange (**MO**) in the presence of aqueous hydrogen peroxide at different irradiation times (irradiation with white light at an irradiance of 150 mW cm^{-2}) of in the presence of **H_2P** (red shape); **ZnP** (green shape); **NPH** (purple shape) and in the absence of any catalyst (Control, blue shape). The band of **MO** was monitored at 464 nm.

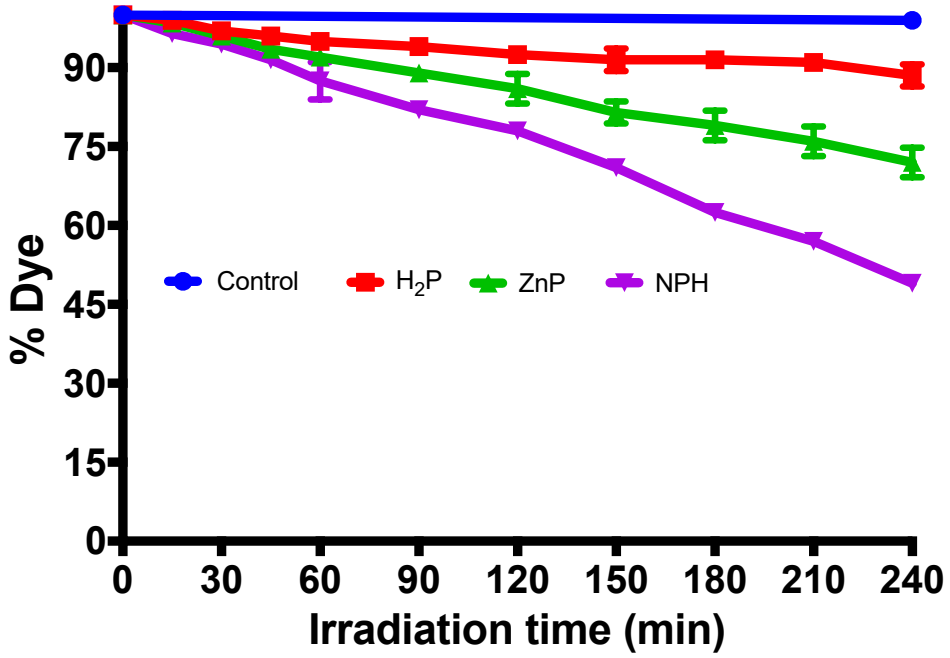

Figure 7. Photocatalytic degradation of methyl orange (**MO**) in the presence of aqueous H_2O_2 and mannitol at different irradiation times (irradiation with white light at an irradiance of 150 mW cm^{-2}) mediated by **H_2P** (red bars), **ZnP** (green bars) and **NPH** (purple bars). The blue bars represent the control reaction (only hydrogen peroxide and mannitol). The band of **MO** was monitored at 464 nm.

In fact, the photocatalytic efficacy of **ZnP** and **NPH** was strongly affected by the presence of mannitol confirming the role of •OH radicals in **MO**

photodegradation (Figure 7). Similar results were obtained for reactions performed with hydrogen peroxide:mannitol (Figure 7) and without hydrogen peroxide (Figure 4). Terephthalic acid (TA) has been used to indirectly measure the production of •OH by fluorescence. The •OH radical species react with terephthalate to yield an intensely fluorescent mono-hydroxylated derivative (HTA). Figure 8 shows the production of HTA from phosphate buffer solution (PBS, pH = 7.0) with H_2O_2 in the presence of **H_2P**, **ZnP** and **NPH** under white light irradiation at different periods of irradiation. Upon irradiation, hydroxyl radicals are produced, yielding a high HTA fluorescence signal. All the photocatalysts are able to generate •OH radical in the presence H_2O_2 and under light, as indicated by the oxidation of the TA probe. Several studies [44] have shown that the TA probe have strong affinity for iron oxide surfaces resulting in lower concentration of the highly fluorescent HTA (Figure 8D). The fluorescence pattern observed for **NPH** in the presence of TA (Figure 8C) is due to the interaction between the nanoparticles' surface and TA. It is worth to mention that in the absence of hydrogen peroxide, the HTA signal is not observed.

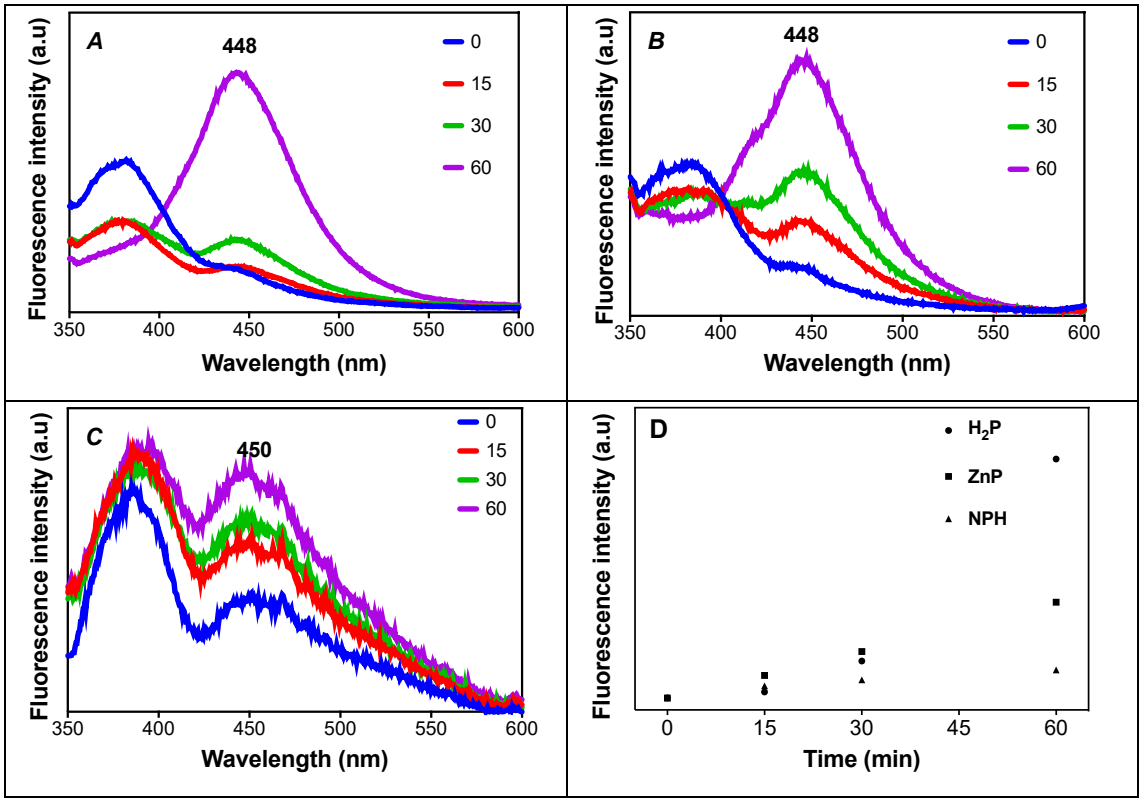

Figure 8. Emission spectra of (A) **H_2P**, (B) **ZnP** and (C) **NPH** solutions in PBS (pH = 7.0) and DMSO (1%) before and after irradiation times (irradiation with white light at an irradiance of 150 mW cm^{-2}) in the presence of aqueous H_2O_2 (λ_{exc} =315 nm) and (D)

Formation of HTA from the photolysis of TA for 60 min in the presence of **H_2P**, **ZnP** and **NPH**.

These results suggest that the photocatalytic mechanism involves mainly two ROS species, namely singlet oxygen and hydroxyl radical. At the end of the photocatalytic reaction using **NPH**, when total degradation of **MO** was observed, fresh solutions of **MO** and H_2O_2 were added to the reaction and subjected to the same reaction conditions of the first use. Again, total degradation of **MO** was observed after 240 min. Indeed, it was possible to efficiently reuse **NPH** at least for three times without loss of catalyst activity.

The photostability and the solubility of the catalyst in solution are important for homogeneous catalysis. The photostability of **H_2P**, **ZnP** and **NPH** were investigated by UV-Vis, monitoring the absorbance of the corresponding Soret band after different times of irradiation. In all cases, a good photostability was observed under the photocatalytic studies conditions.

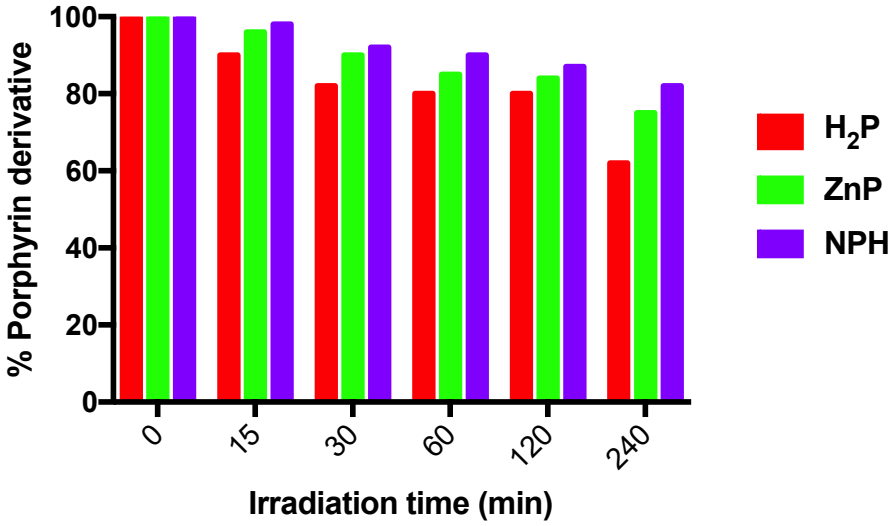

Figure 9. UV-Vis spectrophotometric study of **H_2P**, **ZnP** and **NPH** at a concentration of 5 μM in DMSO/water before and after white light irradiation at an irradiance of 150 mW cm^{-2} at different times (0 - 240 min) using the same conditions of photocatalytic studies.

Conclusions

Core-shell magnetite-silica nanoparticles decorated with a porphyrin bearing *meso*-aryl groups with *N*-tosylethylenediamine residues can be considered for application as excellent photocatalyst for dyes degradation. The

NPH material turned out to be the most effective photocatalyst when compared with the porphyrin precursors in solution. Additionally, the photocatalytic activity can be improved with the addition of aqueous hydrogen peroxide. In this case, two mechanisms (type I and type II) can be involved in the **MO** photodegradation. The efficacy of this new material in the photodegradation of other dyes will be evaluated in future work, together with additional studies for the identification of the reactive species involved in the photocatalysis.

Acknowledgements

Thanks are due to CNPq (Conselho Nacional de Desenvolvimento Científico e Tecnológico) and CAPES (Coordenação de Aperfeiçoamento de Pessoal de Nível Superior). The authors also acknowledge the University of Aveiro and FCT/MCTES (Fundação para a Ciência e Tecnologia and Ministério da Ciência, Tecnologia e Ensino Superior) and European Union (COMPETE and FEDER programs) for the financial support of UIDB/50006/2020 (LAQV-REQUIMTE), UIDB/50011/2020 & UIDP/50011/2020 (CICECO) and UIDB/00100/2020 (CQE) research units and to the project COP2P (PTDC/QUI-QOR/30771/2017), through national funds and, when applicable, co-financed by FEDER–Operational Thematic Program for Competitiveness and Internationalization-COMPETE 2020, within the PT2020 Partnership Agreement. K. A. D. F. Castro thanks CNPq for her post-doctoral scholarship (Process 201107/2014-7) and J. M. M. Rodrigues acknowledges funding in the form of a Junior Researcher Contract under the scope of the project COP2P (PTDC/QUI-QOR/30771/2017).

References

[1] P. Zucca, C.M.B. Neves, M.M.Q. Simões, M.G.P.M.S. Neves, G. Cocco, E. Sanjust, Immobilized Lignin Peroxidase-Like Metalloporphyrins as Reusable Catalysts in Oxidative Bleaching of Industrial Dyes, Molecules 21(7) (2016) 964.
[2] M. Bartolomeu, M. Neves, M.A.F. Faustino, A. Almeida, Wastewater chemical contaminants: remediation by advanced oxidation processes, Photochem. Photobiol. Sci. 17(11) (2018) 1573-1598.
[3] M.A. Al-Ghouti, M.A.M. Khraisheh, S.J. Allen, M.N. Ahmad, The removal of dyes from textile wastewater: a study of the physical characteristics and adsorption mechanisms of diatomaceous earth, J. Environ. Manag. 69(3) (2003) 229-238.
[4] R. Bonnett, M.A. Krysteva, I.G. Lalov, S.V. Artarsky, Water disinfection using photosensitizers immobilized on chitosan, Water Res. 40(6) (2006) 1269-75.

[5] T.K. Saha, H. Frauendorf, M. John, S. Dechert, F. Meyer, Efficient Oxidative Degradation of Azo Dyes by a Water-Soluble Manganese Porphyrin Catalyst, ChemCatChem 5(3) (2013) 796-805.
[6] W. Przystas, E. Zablocka-Godlewska, E. Grabinska-Sota, Efficiency of decolorization of different dyes using fungal biomass immobilized on different solid supports, Braz. J. Microbiol. 49(2) (2018) 285-295.
[7] S. Farias, D. Oliveira, A.A.U. Souza, S.M.A.G.U. Souza, A.F. Morgado, Removal of reactive blue 21 and reactive red 195 dyes using horseradish peroxidase as catalyst, Braz. J. Chem. Eng. 34 (2017) 701-707.
[8] C. Galindo, P. Jacques, A. Kalt, Photodegradation of the aminoazobenzene acid orange 52 by three advanced oxidation processes: UV/H2O2, UV/TiO2 and VIS/TiO2: Comparative mechanistic and kinetic investigations, J. Photochem. Photobiol. A 130(1) (2000) 35-47.
[9] R. Raliya, C. Avery, S. Chakrabarti, P. Biswas, Photocatalytic degradation of methyl orange dye by pristine titanium dioxide, zinc oxide, and graphene oxide nanostructures and their composites under visible light irradiation, Appl. Nanosci. 7(5) (2017) 253-259.
[10] V.P. Barros, M.D. Assis, Iron porphyrins as biomimetical models for disperse azo dye oxidation, J. Braz. Chem. Soc. 24 (2013) 830-836.
[11] K.A.D.F. Castro, S. Silva, P.M. Pereira, M.M.Q. Simões, M.G.P.M.S. Neves, J.A.S. Cavaleiro, F. Wypych, J.P. Tomé, S. Nakagaki, Galactodendritic porphyrinic conjugates as new biomimetic catalysts for oxidation reactions, Inorg. Chem. 54(9) (2015) 4382-93.
[12] S. Nakagaki, K.A.D.F. Castro, M.G.P.M.S. Neves, M.A. Faustino, Y. Iamamoto, The Research on Porphyrins and Analogues in Brazil: A Small Review Covering Catalytic and other Applications since the Beginning at Universidade de São Paulo in Ribeirão Preto until the Joint Venture between Brazilian Researchers and Colleagues from Universidade de Aveiro, Portugal, J. Braz. Chem. Soc. 00 (2019) 1-35.
[13] M.M.Q. Simões, I.C.M.S. Santos, M.G.P.M.S. Neves, A.M.V. Cavaleiro, J.A.S. Cavaleiro, Functionalization of sp2 and sp3 Carbon Centers Catalyzed by Polyoxometalates and Metalloporphyrins, in: A.J.L. Pombeiro (Ed.), Advances in Organometallic Chemistry and Catalysis2013, pp. 59-71.
[14] K.C.M. Westrup, R.M. da Silva, K.M. Mantovani, L. Bach, J.F. Stival, P.G.P. Zamora, F. Wypych, G.S. Machado, S. Nakagaki, Light-assisted cyclohexane oxidation catalysis by a manganese(III) porphyrin immobilized onto zinc hydroxide salt and zinc oxide obtained by zinc hydroxide salt hydrothermal decomposition, Appl. Catal. A 602 (2020) 117708.
[15] M.M.Q. Simões, S.M.G. Pires, M.G.P.M.S. Neves, J.A.S. Cavaleiro, Oxidative Transformations of Organic Compounds Mediated by Metalloporphyrins as Catalysts, Handbook of Porphyrin Science, pp. 197-306.
[16] S.L.H. Rebelo, A.M.N. Silva, C.J. Medforth, C. Freire, Iron(III) Fluorinated Porphyrins: Greener Chemistry from Synthesis to Oxidative Catalysis Reactions, Molecules 21(4) (2016).
[17] F.S. Vinhado, M.E.F. Gandini, Y. Iamamoto, A.M.G. Silva, M.M.Q. Simões, M.G.P.M.S. Neves, A.C. Tomé, S.L.H. Rebelo, A.M.V.M. Pereira, J.A.S. Cavaleiro, Novel Mn(III)chlorins as versatile catalysts for oxyfunctionalisation of hydrocarbons under homogeneous conditions, J. Mol. Catal. A Chem. 239(1-2) (2005) 138-143.
[18] S.L.H. Rebelo, S.M.G. Pires, M.M.Q. Simões, C.J. Medforth, J.A.S. Cavaleiro, M.G.P.M.S. Neves, A Green and Versatile Route to Highly Functionalized Benzofuran Derivatives Using Biomimetic Oxygenation, ChemistrySelect 3(5) (2018) 1392-1403.
[19] S.M.G. Pires, M.M.Q. Simões, I.C.M.S. Santos, S.L.H. Rebelo, M.M. Pereira, M.G.P.M.S. Neves, J.A.S. Cavaleiro, Biomimetic oxidation of organosulfur compounds with hydrogen peroxide catalyzed by manganese porphyrins, Appl. Catal. A 439-440 (2012) 51-56.

[20] S.L.H. Rebelo, M.M.Q. Simões, M.G.P.M.S. Neves, A.M.S. Silva, J.A.S. Cavaleiro, An efficient approach for aromatic epoxidation using hydrogen peroxide and Mn(iii) porphyrins, Chem. Commun. (5) (2004) 608-609.
[21] K.A.D.F. Castro, G.T.P. Brancini, L.D. Costa, J. Biazzoto, M.A. Faustino, A. Tomé, M.d.G.P.M.S. Neves, A. Almeida, M.R. Hamblin, R. Santana da Silva, G. Braga, Efficient photodynamic inactivation of Candida albicans by a porphyrin and potassium iodide co-encapsulated in micelles, Photochem. Photobiol. Sci. (2020).
[22] L.D. Costa, A. e Silva Jde, S.M. Fonseca, C.T. Arranja, A.M. Urbano, A.J. Sobral, Photophysical Characterization and in Vitro Phototoxicity Evaluation of 5,10,15,20-Tetra(quinolin-2-yl)porphyrin as a Potential Sensitizer for Photodynamic Therapy, Molecules 21(4) (2016) 439.
[23] K.A.D.F. Castro, N.M.M. Moura, M.M.Q. Simões, J.A.S. Cavaleiro, M.A.F. Faustino, Â. Cunha, F.A. Almeida Paz, R.F. Mendes, A. Almeida, C.S.R. Freire, C. Vilela, A.J.D. Silvestre, S. Nakagaki, M.G.P.M.S. Neves, Synthesis and characterization of photoactive porphyrin and poly(2-hydroxyethyl methacrylate) based materials with bactericidal properties, Appl. Mater. Today 16 (2019) 332-341.
[24] R.W. Redmond, J.N. Gamlin, A compilation of singlet oxygen yields from biologically relevant molecules, Photochem. Photobiol. 70(4) (1999) 391-475.
[25] J.C. Barona-Castaño, C.C. Carmona-Vargas, T.J. Brocksom, K.T. de Oliveira, Porphyrins as Catalysts in Scalable Organic Reactions, Molecules (Basel, Switzerland) 21(3) (2016) 310-310.
[26] C.M.B. Neves, O.M.S. Filipe, N. Mota, S.A.O. Santos, A.J.D. Silvestre, E.B.H. Santos, M.G.P.M.S. Neves, M.M.Q. Simões, Photodegradation of metoprolol using a porphyrin as photosensitizer under homogeneous and heterogeneous conditions, J. Hazard Mater. 370 (2019) 13-23.
[27] L. Fernandez, V.I. Esteves, A. Cunha, R.J. Schneider, J.P.C. Tomé, Photodegradation of organic pollutants in water by immobilized porphyrins and phthalocyanines, J. Porphyrins Phthalocyanines 20(1-4) (2016) 150-166.
[28] O.M.S. Filipe, E.B.H. Santos, M. Otero, E.A.C. Gonçalves, M.G.P.M.S. Neves, Photodegradation of metoprolol in the presence of aquatic fulvic acids. Kinetic studies, degradation pathways and role of singlet oxygen, OH radicals and fulvic acids triplet states, J. Hazard. Mater. 385 (2020) 121523.
[29] H. He, Y. Zhong, X. Liang, W. Tan, J. Zhu, C.Y. Wang, Natural Magnetite: an efficient catalyst for the degradation of organic contaminant, Sci. Rep. 5 (2015) 10139.
[30] M. Godoi, D.G. Liz, E.W. Ricardo, M.S.T. Rocha, J.B. Azeredo, A.L. Braga, Magnetite (Fe3O4) nanoparticles: an efficient and recoverable catalyst for the synthesis of alkynyl chalcogenides (selenides and tellurides) from terminal acetylenes and diorganyl dichalcogenides, Tetrahedron 70(20) (2014) 3349-3354.
[31] H. Alina Maria, G. Alexandru Mihai, G. Monica Cartelle, M. Laurentiu, M. George Dan, Novel Drug Delivery Magnetite Nano-systems Used in Antimicrobial Therapy, Curr. Org. Chem. 18(2) (2014) 185-191.
[32] G. Unsoy, U. Gunduz, O. Oprea, D. Ficai, M. Sonmez, M. Radulescu, M. Alexie, A. Ficai, Magnetite: from synthesis to applications, Curr. Top. Med. Chem. 15(16) (2015) 1622-40.
[33] I.L. Ardelean, L.B.N. Stoencea, D. Ficai, A. Ficai, R. Trusca, B.S. Vasile, G. Nechifor, E. Andronescu, Development of Stabilized Magnetite Nanoparticles for Medical Applications, J. Nanomater. 2017 (2017) 9.
[34] J. Chang, Q. Zhang, Y. Liu, Y. Shi, Z. Qin, Preparation of Fe3O4/TiO2 magnetic photocatalyst for photocatalytic degradation of phenol, J. Mater. Sci. Mater. Electron. 29(10) (2018) 8258-8266.
[35] K.-H. Choi, K.-K. Wang, E.P. Shin, S.-L. Oh, J.-S. Jung, H.-K. Kim, Y.-R. Kim, Water-Soluble Magnetic Nanoparticles Functionalized with Photosensitizer for Photocatalytic Application, J. Phys. Chem. C 115(8) (2011) 3212-3219.
[36] M. Neamţu, C. Nădejde, V.D. Hodoroaba, R.J. Schneider, U. Panne, Singlet oxygen generation potential of porphyrin-sensitized magnetite nanoparticles:

Synthesis, characterization and photocatalytic application, Appl. Catal. B: Environ. 232 (2018) 553-561.
[37] A.M.d.A.R. Gonsalves, J.M.T.B. Varejão, M.M. Pereira, Some new aspects related to the synthesis of meso-substituted porphyrins, J. Heterocycl. Chem. 28(3) (1991) 635-640.
[38] J.M. Rodrigues, A.S. Farinha, P.V. Muteto, S.M. Woranovicz-Barreira, F.A. Almeida Paz, M.G.P.M.S. Neves, J.A. Cavaleiro, A.C. Tomé, M.T. Gomes, J.L. Sessler, J.P.C. Tomé, New porphyrin derivatives for phosphate anion sensing in both organic and aqueous media, Chem. Commun. 50(11) (2014) 1359-61.
[39] C.M.B. Carvalho, E. Alves, L. Costa, J.P.C. Tomé, M.A.F. Faustino, M.G.P.M.S. Neves, A.C. Tomé, J.A.S. Cavaleiro, A. Almeida, Â. Cunha, Z. Lin, J. Rocha, Functional cationic nanomagnet-porphyrin hybrids for the photoinactivation of microorganisms, ACS Nano 4(12) (2010) 7133-40.
[40] P. Battioni, E. Cardin, M. Louloudi, B. Schöllhorn, G.A. Spyroulias, D. Mansuy, T.G. Traylor, Metalloporphyrinosilicas: a new class of hybrid organic–inorganic materials acting as selective biomimetic oxidation catalysts, Chem. Commun. (17) (1996) 2037-2038.
[41] J.L. Clark, J.E. Hill, I.D. Rettig, J.J. Beres, R. Ziniuk, T.Y. Ohulchanskyy, T.M. McCormick, M.R. Detty, Importance of Singlet Oxygen in Photocatalytic Reactions of 2-Aryl-1,2,3,4-tetrahydroisoquinolines Using Chalcogenorosamine Photocatalysts, Organometallics 38(12) (2019) 2431-2442.
[42] W. Spiller, H. Kliesch, D. Wöhrle, S. Hackbarth, B. Röder, G. Schnurpfeil, Singlet oxygen quantum yields of different photosensitizers in polar solvents and micellar solutions, J. Porphyrins Phthalocyanines 2(2) (1998) 145-158.
[43] M.Q. Mesquita, J.C.J.M.D.S. Menezes, S.M.G. Pires, M.G.P.M.S. Neves, M.M.Q. Simões, A.C. Tomé, J.A.S. Cavaleiro, Â. Cunha, A.L. Daniel-da-Silva, A. Almeida, M.A.F. Faustino, Pyrrolidine-fused chlorin photosensitizer immobilized on solid supports for the photoinactivation of Gram negative bacteria, Dyes Pigments 110 (2014) 123-133.
[44] G. Lyngsie, L. Krumina, A. Tunlid, P. Persson, Generation of hydroxyl radicals from reactions between a dimethoxyhydroquinone and iron oxide nanoparticles, Sci. Rep. 8(1) (2018) 10834.
[45] B. Shen, R.G. Jensen, H.J. Bohnert, Mannitol Protects against Oxidation by Hydroxyl Radicals, Plant Physiol 115(2) (1997) 527-532.